

# Active Vibration Control of a PZT Actuated Suspension in Hard Disk Drives<sup>1</sup>

Yunfeng Li and Roberto Horowitz  
Computer Mechanics Laboratory (CML)  
Department of Mechanical Engineering

University of California at Berkeley, CA 94720-1740

yunfeng@me.berkeley.edu, horowitz@me.berkeley.edu

## Abstract

This paper presents the design and testing results of active vibration control for a PZT actuated suspension. One PZT strip on the suspension is used as a vibration sensor, and the other as an actuator. A state space model for the PZT actuated suspension was established based on curve-fitted transfer functions, and a feedback damping controller was designed, using the  $H_\infty$  controller design method to minimize the peak magnitude of the closed loop transfer function frequency response. An experimental verification of the control scheme was performed. In the experiment, the RMS value of off-track motion due to air-flow excited suspension vibration in the 4-16 kHz range was reduced from 6.0 nm to 3.5 nm for 7200 RPM spindle rotation speed (42% reduction), and from 9.8 nm to 5.9 nm for 10K RPM spindle rotation speed (40% reduction).

## 1 Introduction

With the continuing increase in storage density and spindle rotation speed in hard disk drives, suspension vibration becomes a significant challenge for achieving the required track mis-registration (TMR) budget. For example, the  $1-\sigma$  TMR budget for 100k tracks-per-inch (TPI) track density is about 8 nm. In our experimental setup, we found the off-track motion of the head due to air-flow excited suspension vibration can be as high as 10 nm for a PZT actuated suspension at 10k RPM spindle rotation speed. Similar results is presented in [1].

For single stage servo systems, active vibration control of the actuator structural resonance modes in disk drives have been reported in [2], [3]. For active suspension vibration control using dual-stage servo systems, strain sensors can be attached on the surface of the suspension to obtain the vibration signal, and the second stage mini/micro actuator can

be used to compensate suspension vibration induced TMR.

The vibration compensation scheme with dual-stage servo systems depends on the type and configuration of the dual-stage actuator. For an actuated slider dual-stage servo system, in which a MEMS microactuator (MA) is positioned at the tip of the suspension and actuates the slider/head directly, the second-stage actuation is in front of the suspension. Adaptive feedforward control techniques can be used so that motion of the MA cancels the suspension vibration [4].

In this paper we discuss vibration compensation for a PZT actuated suspension dual-stage servo system. PZT actuated suspensions usually are designed to have a relative soft sway mode, in order to obtain large DC gain. This makes the PZT actuated suspension more susceptible to the air-flow excitation, when compared to conventional suspensions. The PZT actuators on the PZT actuated suspension are located behind the suspension vibration modes. Thus, a feedback damping control scheme can be utilized to suppress air-flow excited suspension vibration.

The PZT can also be used as a piezoelectric strain sensor. In our test, the damping controller was implemented using one of the two PZT strips on the suspension as a vibration sensor and the other one as an actuator. A damping controller, which was designed using the  $H_\infty$  control design method was tested with the PZT actuated suspension mounted on a spin stand.

Section 1 of the paper describes the test setup and vibration sensing scheme using the PZT. Section 2 presents the control system model and damping controller design using  $H_\infty$  design method. Experimental results are provided in section 3. The last section is conclusions.

## 2 Sensing of Air-Flow Excited Suspension Vibration

### 2.1 Test Setup

Fig. 1 is a picture of our experimental setup. A PZT actuated suspension, manufactured by Hutchinson Technology Inc. (HTI), was mounted on a spin stand. The displacement

<sup>1</sup>Research supported by the National Storage Industry Consortium (NSIC) and the Computer Mechanics Laboratory (CML) of U.C. Berkeley.

of the slider was measured using a laser Doppler vibrometer (LDV) and monitored with an HP digital analyzer.

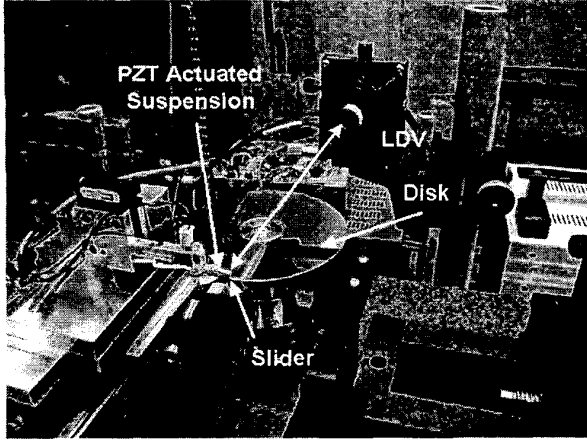


Figure 1: A photograph of the experimentl setup

The PZT actuated suspension has two PZT strips located near the root of the suspension. They generate a push-pull action and bend the suspension to actuate the slider located at the tip of the suspension. When a mechanical stress is applied to a piezoelectric material, such as PZT, it will generate charge. Thus, the PZT can also be used as a strain sensor. In our test, we used one PZT strip on the suspension as a vibration sensor, and only one PZT was used as an actuator. As a result, the actuation gain and stroke limit of the PZT actuated suspension are reduced by half. However, the stroke limit ( $\pm 0.6\mu\text{m}$  for  $\pm 40\text{V}$  input voltage in this case) is still much larger than what is required for track-following control.

## 2.2 Sensing of Air-Flow Excited Suspension Vibration Using PZT

The slider motion due to air-flow excited suspension vibration is in the nano-meter range. Thus, the vibration sensor needs to have a large sensitivity to pick up this small signal. First, we will estimate the sensitivity of the PZT sensor. The charge density on the surface of the PZT sensor when it is subjected to a stress in the transverse direction is [5]

$$P_3 = d_{31}\sigma_1, \quad (1)$$

where  $P_3$  is the charge density,  $\sigma_1$  is the stress, and  $d_{31}$  is a charge constant with units Coulomb/Newton. The stress is giving by

$$\sigma_1 = E\varepsilon_1, \quad (2)$$

where  $E$  is the Young's modulus and  $\varepsilon_1$  is the strain. The capacitance of a PZT trip is

$$C = \varepsilon_r \varepsilon_0 \frac{w * l}{t}, \quad (3)$$

where  $\varepsilon_r$  is the relative permittivity of PZT,  $\varepsilon_0$  is permittivity of vacuum and  $w, l, t$  are respectively the width, length and height of the PZT strip. Thus, the output voltage of a PZT strip, subjected to a strain  $\varepsilon_1$ , is

$$V = \frac{Q}{C} = \frac{d_{31}Et}{\varepsilon_r \varepsilon_0} \varepsilon_1. \quad (4)$$

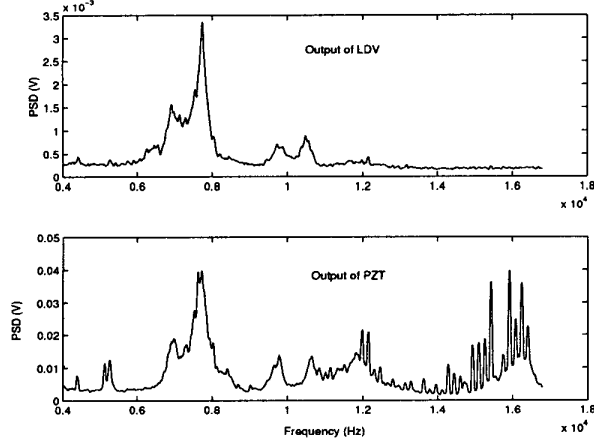
For the PZT strip used on our PZT actuated suspension,  $d_{31} = 110\text{e} - 12\text{C/N}$ ,  $E = 83\text{GPa}$ ,  $\varepsilon_r = 1700$ , and  $t = 0.25\text{mm}$ , the voltage output gain was calculated to be  $0.15\text{ mV/nano-strain}$ . If we approximate the PZT actuated suspension as a mechanical leverage from PZT stretch to the tip lateral motion with a gain of 8, and the length of the PZT strip is  $4\text{mm}$ , we can further calculate the gain from the slider lateral motion to the PZT output voltage to be  $4.5\text{ mV/nm}$ . In our experiments, we observed that this gain was about  $1\text{ mV/nm}$ . The discrepancy between the estimated and actual value is probably due to the fact that some factors, such as parasitic capacitance of the wires and the input capacitance of the amplifier were not accounted for in the derivations that lead to Eq. (4) when calculate the output voltage. In a separate test, we glued a semiconductor piezoresistive strain gauge, which has a gauge factor of 150, on the suspension's load beam. We found the sensitivity of the PZT sensor is much larger than that of the semiconductor strain sensor we tested.

The vibration sensor must be able to pick up the vibration modes that have largest contributions to the off-track motion of the slider. Fig. 2 compares the power spectrum density (PSD) of the slider motion measured using an LDV and the PZT sensor output. The upper part of Fig. 2 is the PSD of the LDV output, while the lower part is the PSD of the PZT output. In this test, the spindle rotation speed is  $10\text{k RPM}$ , and the suspension is located at the outer diameter (OD) of the disk. We can see the PZT sensor output has a very strong correlation with the slider off-track motion. It picks up most of the major off-track modes below  $12\text{ kHz}$ . At higher frequencies, the PZT sensor amplifies the vibration signal due to the existence of an anti-resonance mode in the sensor's transfer function, as will be discussed in section 3.1.

## 3 Control System Models and Vibration Control Design

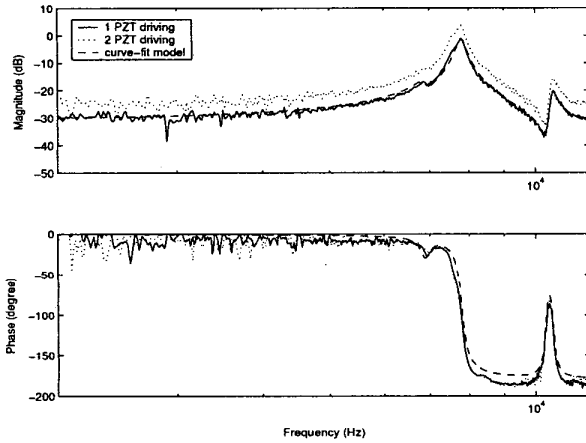
### 3.1 Actuator and Sensor Models

Fig. 3 shows the measured frequency responses from a voltage input to the PZT actuator to the slider lateral motion, as measured by the LDV. The dot line in Fig. 3 is when both PZT trips are used for actuation, while the solid line is when only one PZT strip is used for actuation. The frequency responses are almost same except the gain is reduced by half ( $6\text{dB}$ ) when using only one PZT trip as an actuator. Thus, unsymmetrically actuation of the suspension when one PZT strip is used did not result in a noticeable detrimental effect on the plant dynamics of the actuated suspension. A model



**Figure 2:** PSD of the outputs of the LDV and the PZT sensor

of the actuator was obtain by curve-fitting the measured frequency response. The dash line in the plot is the simulated frequency response of this model.



**Figure 3:** Frequency response of the PZT actuator

The transfer function of the actuator model includes three modes

$$G_A(s) = g_{dc}G_{A1}(s)G_{A2}(s)G_{A3}(s), \quad (5)$$

where the DC gain,  $g_{dc} = 15nm/V$ .  $G_{A1}(s)$  is a suspension sway mode

$$G_{A1} = \frac{\omega_1^2}{s^2 + 2\zeta_1\omega_1 + \omega_1^2} \quad (6)$$

with resonance frequency  $\omega_1 = 7.8kHz$ , and damping factor  $\zeta_1 = 0.02$ .  $G_{A2}$  is a torsional mode near 6.8 kHz, and  $G_{A3}$  is another torsional mode near 10.5 kHz.

Fig. 4 is the frequency response from slider displacement, as measured by the LDV, to the PZT sensor output when the

PZT actuator is driven with a sweep sine. The solid line in Fig. 4 is the measured response, while the dash line is the response of a curve-fitted model. The transfer function of the sensor model is

$$G_S(s) = g_s G_{S1}(s)G_{S2}(s), \quad (7)$$

where  $g_s$  is the DC gain, and  $G_{S1}$  is an anti-resonance mode

$$G_{S1} = \frac{s^2 + 2\zeta_2\omega_2 + \omega_2^2}{\omega_2^2} \quad (8)$$

with  $\omega_2 = 6.35kHz$ , and  $\zeta_2 = 0.008$ .  $G_{S2}$  is a torsional mode near 10.5 kHz.

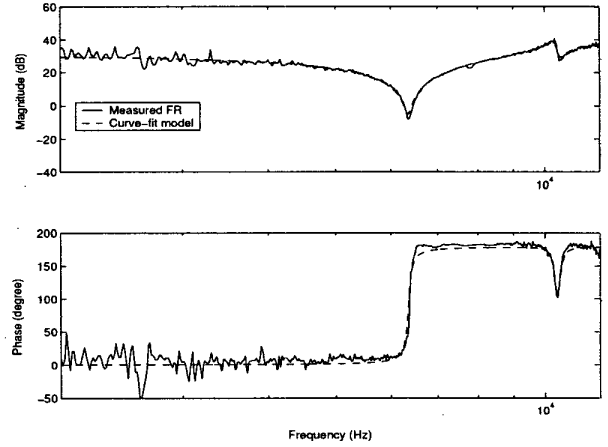


**Figure 4:** Frequency response of the PZT sensor

From the frequency response plot in Fig. 4 we notice that the sensor amplifies signal at the high frequency because of the anti-resonance mode. This explains why there are some high frequency resonance peaks amplified in the power spectrum density of the sensor output in Fig 2.

Fig. 5 shows the frequency responses from the PZT actuator voltage input to the PZT sensor voltage output. The solid line is the measured response, while the dash line is a model, given by the following transfer function

$$G_{AS}(s) = G_A(s)G_S(s), \quad (9)$$

where  $G_A(s)$  and  $G_S(s)$  are respectively defined in Eq. (5) and Eq. (7).

### 3.2 Vibration Control Design

In order to perform a controller design using an optimal control design methodology such as LQG or  $H_\infty$ , we need to formulate a one-input-two-output state space model of the PZT actuated suspension and sensor, and relate the states of the system to the displacement of the slider and the PZT sensor output. Comparing Fig. 2 and Fig. 3, we can see that the most significant off-track mode which is excited by

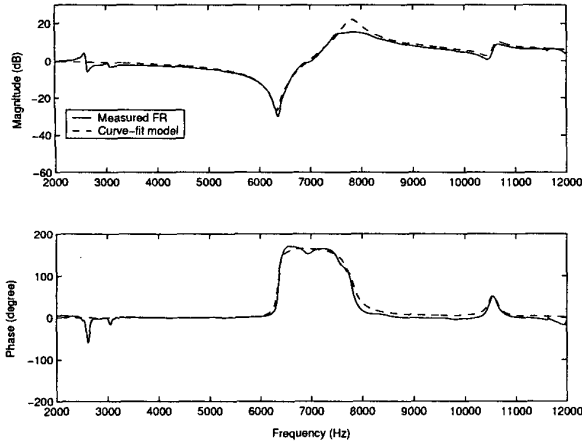


Figure 5: Frequency response from the PZT actuator to the PZT sensor

the air-flow is the sway mode. To simplify the controller design, the torsional modes of the suspension were neglected in the control plant and sensor state space model. Thus, the model only includes the sway mode of the actuator, as defined in Eq. (6), and the anti-resonance mode of the sensor, as defined in Eq. (8).

A state equation of the system can be written as

$$\begin{bmatrix} \dot{x}_1 \\ \dot{x}_2 \end{bmatrix} = \begin{bmatrix} 0 & 1 \\ a_{21} & a_{22} \end{bmatrix} \begin{bmatrix} x_1 \\ x_2 \end{bmatrix} + \begin{bmatrix} 0 \\ 1 \end{bmatrix} u, \quad (10)$$

where

$$a_{21} = -\omega_1^2 \quad (11)$$

$$a_{22} = -2\zeta_1\omega_1. \quad (12)$$

The corresponding output equation is

$$\begin{bmatrix} y \\ z \end{bmatrix} = \begin{bmatrix} \omega_1^2 & 0 \\ c_{21} & c_{22} \end{bmatrix} \begin{bmatrix} x_1 \\ x_2 \end{bmatrix} + \begin{bmatrix} 0 \\ w_1^2/w_2^2 \end{bmatrix} u, \quad (13)$$

where  $y$  is the displacement of the slider,  $z$  is the PZT sensor output, and

$$c_{21} = w_1^2(w_2^2 - w_1^2)/w_2^2 \quad (14)$$

$$c_{22} = w_1^2(2\zeta_2\omega_2 - 2\zeta_1\omega_1)/w_2^2. \quad (15)$$

Fig. 6 is a block diagram that was used in the  $H_\infty$  controller design. In the block diagram,  $P$  represents the PZT actuated suspension plant.  $y$  is the displacement of the slider, while  $z$  is the PZT sensor output.  $n$  is the sensor measurement noise. Windage disturbance was modelled to be a torque disturbance  $d$  acting at the input of the PZT actuator.  $u_c$  is a outer loop control signal generated by the dual-stage servo controller. In this paper, we did not consider the outer servo feedback loop, and set  $u_c = 0$ .  $K$  is the vibration damping controller to be synthesized, and  $u$  is the output of  $K$ .

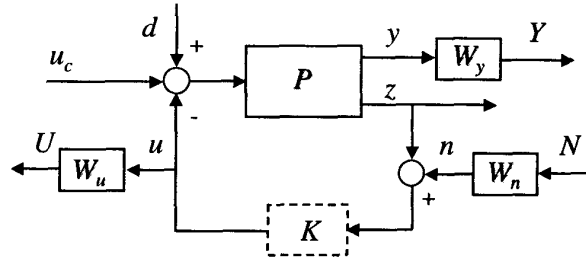


Figure 6:  $H_\infty$  controller design block diagram

Weighting function  $W_n$  was used to characterize the measurement noise, which was assumed to be 5mV by letting  $W_n = 0.005$ .  $W_u$  was used to bound the control voltage input. A constant  $W_u = 1$  was used to limit the control input within  $\pm 1V$ .  $W_y$  was selected to bound the closed loop frequency response from  $d$  to  $y$ ,  $G_y$  (the transfer function from  $u_c$  to  $y$  is the same). We choose  $W_y$  to be

$$W_y = \frac{1}{g_{dc}}, \quad (16)$$

where  $g_{dc}$  is the DC gain of the PZT actuator. Suppose the  $H_\infty$  norm of the closed loop system is  $\beta$ , then we have

$$\|G_y\|_\infty \leq \frac{\beta}{\|W_y\|_\infty} = \beta g_{dc}. \quad (17)$$

Thus, the design objective is to bound the peak in the magnitude of the frequency response of  $G_y$  within the DC gain of the PZT actuator.

The controller was generated using *hinfsyn* function of the  $\mu$ -tools Matlab toolbox [6]. The  $H_\infty$  norm in the resulting design is  $\beta = 1.07$ . The resulting closed loop frequency response from  $d$  to  $y$ , with the loop closed from  $z$  to  $u$  using the generated controller is shown as the dash line in Fig. 7. The magnitude of the frequency response is almost flat up to 5 kHz, then it slowly goes down, with the resonance mode being well damped.

Fig. 8 shows the open loop frequency response of the transfer function from the input of the damping controller to  $z$ . The gain margin is infinite, and the phase margin is  $91^\circ$ . Thus the controller is robust in terms of gain and phase margins. Fig. 9 shows the closed loop frequency response for  $d$  to  $z$

The synthesized controller has two poles to cancel the anti-resonance zeros of the sensor and a zero near 1.5 Hz. The zero acts as a D-action at high frequency to increase the damping. Fig. 10 is the Bode plot of controller.

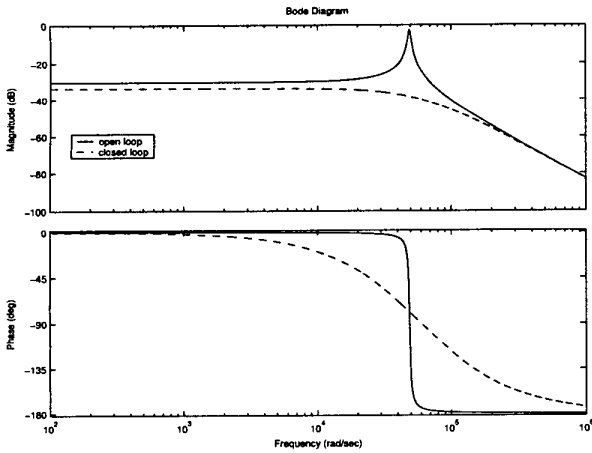


Figure 7: Closed loop frequency response of the displacement output

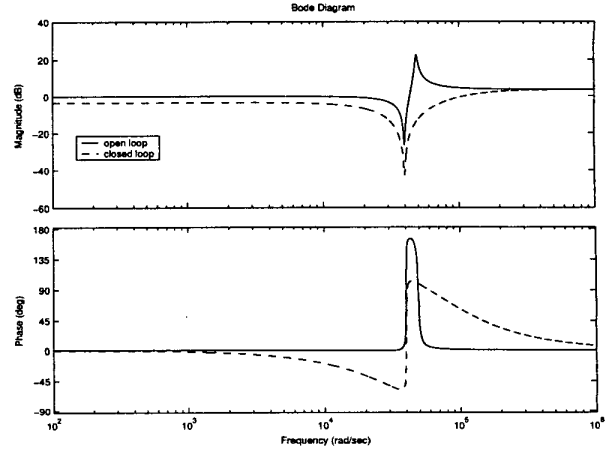


Figure 9: Closed loop frequency response of the sensor output

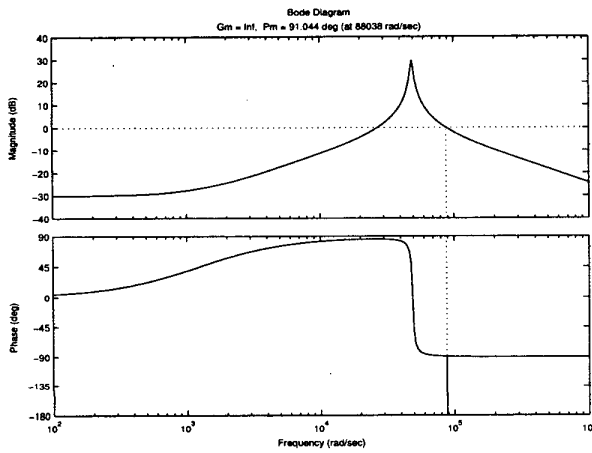


Figure 8: Open loop frequency response

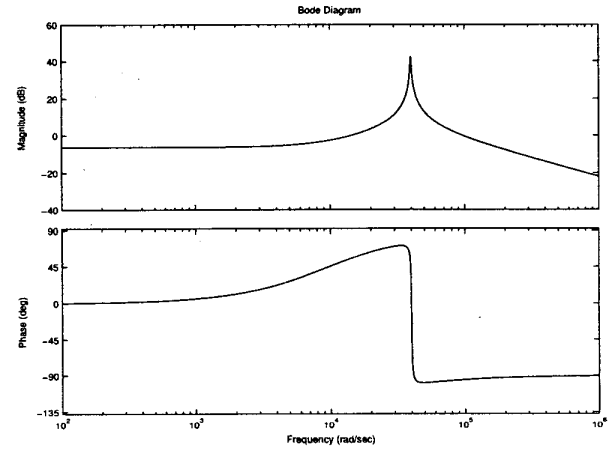


Figure 10: Bode plot of the controller

#### 4 Experimental Results

The synthesized controller was discretized and implemented using a Texas Instrument TMS320C6711 floating-point DSP. The sampling frequency was chosen to be 100 kHz. In the experiment, the suspension is located at the OD of the disk, where the windage excitation is expected to be the biggest. Fig. 11 shows the power spectrum density of the slider off-track motion, as measured by an LDV, when the spindle rotation speed is 7200 RPM. The upper half plot is when damping control is not applied, while the lower half plot is when damping control is applied. We can see air-flow excited suspension vibration is greatly attenuated. The RMS value of slider motion due to suspension vibration in the 4-16 kHz range is reduced from 6.0nm to 3.5nm, which represents a 42% reduction. Fig. 12 is the test result for 10k RPM spindle rotation speed. In this case, the RMS value of

off-track motion due to air-flow excited suspension vibration in the 4-16 kHz range is reduced from 9.8nm to 5.9nm, which is a reduction of 40%.

#### 5 Conclusions

Tests have shown that PZT is a feasible candidate for vibration sensing in a PZT actuated suspension, and feedback damping control is effective in suppressing slider off-track motion due to air-flow excitation for a PZT actuated suspension. The dynamic response of the PZT actuated suspension can also be greatly improved with the use of the damping controller. Thus, potentially a higher servo bandwidth can be achieved for PZT actuated suspension dual-stage servo system.

The test data also shows the damping controller is most effective in attenuating the sway mode vibration of the sus-

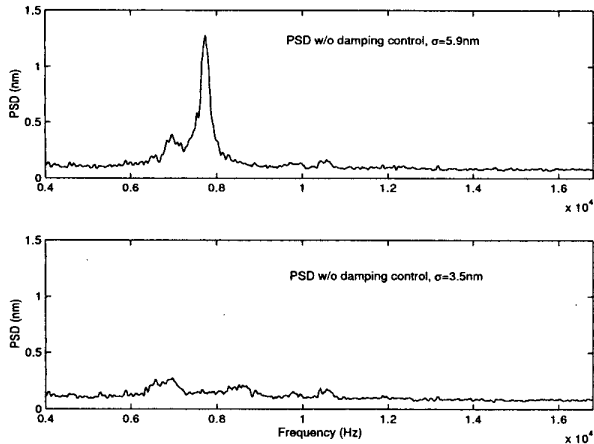


**Figure 11:** Power spectrum density of the slider motion (7200 RPM)

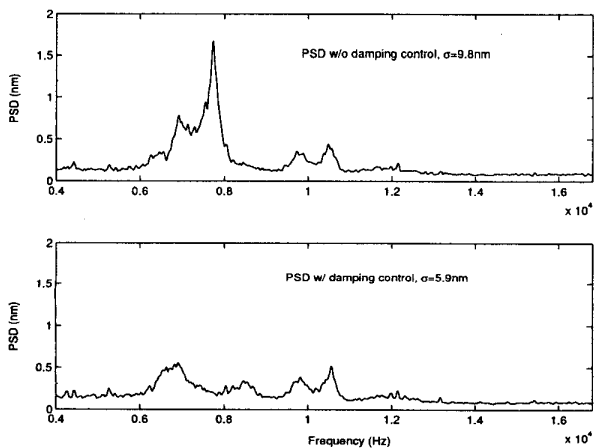


**Figure 12:** Power spectrum density of the slider motion (10k RPM)

pension, but is less effective for suppressing the torsional modes vibration. One possible future work is to use a scheme similar to the one presented in [7] to incorporate an additional minimum variance adaptive feedforward control loop to suppress the left-over vibration modes by the damping controller.

### Acknowledgments

The authors thank Robert Evans from HTI for providing us pre-production test samples and useful discussions. They also thank the industrial participants of the NSIC EHDR servo team for their comments and useful discussions.

### References

- [1] M.W. Davis, "A New Spin on Suspension Windage", *Insight*, March/April 2001
- [2] Y. Huang, M. Banther, P.D. Mathur, W.C. Messner, "Design and Analysis of a High Bandwidth Disk Drive Servo System Using an Instrumented Suspension", *IEEE/ASME transaction of Mechatronics*, Vol. 4, No. 2, June 1999
- [3] F.-Y. Huang, W. Imano, T. Semba, F. Lee, "Rotary Actuator Dynamics with Active Damping", *11th Annual Symposium on Information Storage and Processing System*, June, 2000
- [4] Y. Li, R. Horowitz, "Active Suspension Vibration Control with Dual Stage Actuators in Hard Disk Drives", *Proceedings of American Automatic Control Conference*, June, 2001
- [5] J. Fraden, "Handbook of modern sensors : physics, designs, and applications", 2nd ed. Woodbury, N.Y. : American Institute of Physics, 1997
- [6] G. J. Balas, J. C. Doyle, K. Glover, A. Packard, R. Smith, "m-Analysis and Synthesis ToolBox," MUSYN Inc. and The MathWorks, Inc., 1995
- [7] R. Horowitz, B. Li, J.W., McCormick, "Wiener filter-based minimum variance self-tuning regulation," *Automatica*, vol.34, (no.5), Elsevier, May 1998